Spectrum Map Construction Method Based on Dynamic Window Size Tensor Ring Low-rank Factors

Yihan HU [1,2,3], Jianzhao ZHANG [2], Yongxiang LIU [2], Guangjie LIU [1,3], Guokai CHEN [2]

[1] Nanjing University of Information Science and Technology, Nanjing, China
[2] The Sixty-Third Research Institute, National University of Defense Technology, Nanjing, China
[3] Key Laboratory of Intelligent Support Technology in Complex Environment, Ministry of Education, Nanjing, China

20211249658@nuist.edu.cn, jianzhao63s@nudt.edu.cn, lyx63s@163.com, gjieliu@nuist.edu.cn, guokai.chen@nudt.edu.cn

Submitted September 17, 2023 / Accepted January 5, 2024 / Online first January 23, 2024

Abstract. *Spectrum maps can model the received signal strength over a geographical region and will play a pivotal role in the intended spectrum management scheme. Traditional spectrum map construction methods cannot fully utilize the spatial-temporal correlation characteristics of observed spectrum data in a time-varying spectrum situation. The computational complexity for real-time scenes is unaffordable, and the current spectrum situation cannot be estimated promptly. To address this problem, we first model the spatial-temporal spectrum data by tensors. Then, based on the low-rank statistical characteristic of the spectrum map, we apply the tensor ring low-rank factors (TRLRF) algorithm to recover the missing spectrum data. Finally, a dynamic window mechanism is introduced to reduce the computational complexity further. The simulation results show that the proposed dynamic window size tensor ring low-rank factors (DW-TRLRF) algorithm yields higher accuracy than other state-of-the-art algorithms with significantly lower complexity.*

Keywords

Spatial-temporal spectrum data, spectrum situation construction, spectrum map, mobile radiation source

1. Introduction

With the popularization of intelligent terminals and the emergence of various new services, spectrum scarcity and low utilization have become bottlenecks hindering the sustainable development of the wireless communication industry [1]. Real-time monitoring of the radio spectrum environment is the premise for optimal allocation and management of spectrum resources [2]. As a visual spectrum resource description tool, a spectrum map maps the received signal strength in the area of interest to the corresponding geographical coordinates, describes the spatial characteristic distribution of the received signal strength [3], [4], and provides essential support for spectrum monitoring, spectrum management, and signal identification. Therefore, spectrum map construction has received extensive attention in academia and industry.

The existing spectrum map construction methods can be divided into two categories based on whether information related to the propagation model is used: parametric and nonparametric methods [5]. Commonly used nonparametric methods include the graph processing method [6], the low-rank matrix completion method [7], and the kriging method [8], and parametric methods include the compressed sensing method [9] and the tensor decomposition method [10]. These methods focus primarily on spectrum map construction in the spatial domain without considering the time-domain variation characteristics of spectrum maps.

To accurately describe the time-space-frequency multidimensional characteristics of spectrum data, two-dimensional spectrum maps must be extended to the multidimensional space, and tensors must be introduced accordingly. A tensor is a multidimensional array, which is an extension of a vector and matrix. It has rich mathematical properties and application potential, and it has been successfully applied in computer vision and image fields [11–13]. Yuan et al. presented in [14] that a tensor ring low-rank factors (TRLRF) algorithm imposes low-rank constraints on potential tensor ring factors by introducing nuclear norm regularization. The alternating direction method of multipliers (ADMM) [15] is adopted to solve the problem, effectively reducing the burden of the rank selection of the tensor ring and reducing the computational complexity. Wang et al. [16] presented a tensor ring completion by alternating least square (TR-ALS) algorithm, which uses alternating minimization in factors represented by matrix product state to restore missing data. In [17], Yuan et al. presented a tensor ring weighted optimization (TR-WOPT) algorithm using the flexibility of tensor ring decomposition, found the latent factors of the incomplete tensor through the gradient descent algorithm, and then used the latent factors to predict the missing items of the tensor. Tang et al. [18] were the first to propose using

DOI: 10.13164/re.2024.0163

spectrum tensors to describe multidimensional spectrum data and proposed a high accuracy low rank tensor completion (HaLRTC) algorithm combined with a prediction model to restore incomplete spectrum information. Tang et al. [19] discussed the construction and analysis of multidimensional spectrum maps from the perspective of tensors, proposed a method based on tensors to process multidimensional spectrum data, and introduced a missing value recovery method based on tensor decomposition. Zhang et al. [20] presented a dynamic window size based canonical polyadic decomposition (DW-CPD) algorithm based on the dynamic spectrum situation generation problem, which uses historical time information to complement the missing spectrum data at the current time.

The traditional spectrum map construction method cannot take advantage of the spatial-temporal correlation characteristics of the observed spectrum data. Therefore, the computational complexity of constructing spectrum maps is challenging to bear using all observed spectrum data. This paper proposes a dynamic window size tensor ring low-rank factors (DW-TRLRF) algorithm to solve this major challenge in constructing spectrum maps. Using the correlation of spatial-temporal spectrum data reduces the computational complexity by solving the data source with a dynamic window mechanism. The main innovations of this paper include the following:

- A spectrum map construction model based on tensor completion is proposed, and a spectrum map construction algorithm based on tensor ring low-rank factors (TRLRF) is designed. The tensor ring factors represented by tensor ring decomposition can be found from incomplete spectrum data observations to estimate missing items in the spectrum data.
- Based on the correlation of spatial-temporal spectrum data, a DW-TRLRF algorithm is proposed to support the requirement of real-time construction of spectrum maps. Observation data in the dynamic window size with solid correlation with the current moment are selected to adapt to the current spectrum situation modeling under the dynamic changes in the electromagnetic spectrum environment.
- Simulation analysis results show that under the typical scenario where the standard deviation of shadow fading is 3 dB and the missing rate of spectrum data is in the range of 0.2–0.8, the root square error (RSE) of the DW-TRLRF algorithm is reduced by 12.41% and 4.54% on average compared with the classic kriging interpolation method and the TRLRF algorithm, respectively. Additionally, the computational complexity is significantly reduced compared with the classic kriging interpolation method and the TRLRF algorithm.

The rest of this paper is organized as follows. Section 2 introduces the scene model of this paper. Section 3 proposes a spectrum map construction algorithm based on DW-TRLRF. Section 4 presents the simulation analysis results. Finally, we conclude the paper in Sec. 5.

2. Problem Modeling

We first briefly introduce the tensor ring decomposition model. We then introduce the problem scenario, and finally, we model the time-varying spectrum map construction as a tensor completion problem.

2.1 Tensor Ring Decomposition Model

Tensor ring decomposition is a model for processing high-dimensional spectrum tensors. It decomposes complex high-dimensional spectrum data into a series of easy-to-handle low-dimensional spectrum data structures in a ring structure, which is useful for extracting valuable features and information. When $n = 1, \cdots, N$, the tensor ring (TR) factors are represented by $\mathcal{G}^{(n)} \in \mathbb{R}^{R_n \times I_n \times R_{n+1}}$. Each factor consists of two rank-modes (mode-1 and mode-3) and a one-dimensional mode (mode-2). The rank of the tensor ring is defined as $rank_{\mathrm{TR}}(\mathcal{X}) = (R_1, R_2, \cdots, R_N)$, where $R_1 = R_2 = \cdots = R_N$, which controls the model complexity of the tensor ring decomposition. Therefore, for a tensor $\mathcal{X} \in \mathbb{R}^{I_1 \times I_2 \cdots \times I_N}$, the tensor ring decomposition is defined as:

$$\mathcal{X}(i_1, i_2, \ldots, i_N) = \mathrm{Trace}\left\{\prod_{n=1}^{N} \mathbf{G}_{i_n}^{(n)}\right\} \tag{1}$$

where $\mathrm{Trace}\{\cdot\}$ is a matrix trace operation, $\mathbf{G}_{i_n}^{(n)} \in \mathbb{R}^{R_n \times R_{n+1}}$ represents the i_nth mode-2 slice matrix of the TR factors $\mathcal{G}^{(n)}$, which can also be represented by $\mathcal{G}^{(n)}(:, i_n, :)$. This tensor ring decomposition model is depicted in Fig. 1.

2.2 Problem Scenario

A group of monitoring sensors and multiple mobile radiation sources are randomly arranged in the target area, where the initial position and emission power of the radiation source are unknown, as shown in Fig. 2.

The position of monitoring sensor i is represented by m_i, and the measured received signal strength is represented by $P(m_i)$ [21]:

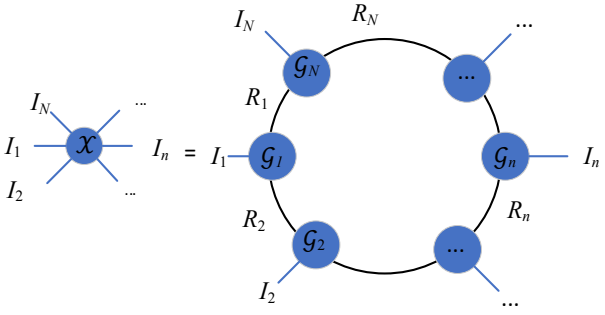

Fig. 1. Tensor ring decomposition model.

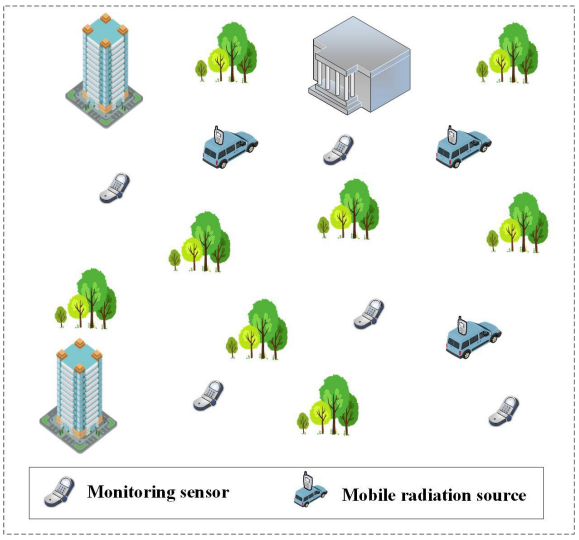

Fig. 2. Schematic diagram of the layout of mobile radiation sources and monitoring sensors in the area.

$$P(m_i) = P_{T_p} - K - 10\varepsilon \log_{10}(\|m_p - m_i\|) + W_{m_i}. \quad (2)$$

In this formula, P_{T_p} is the emission power of a certain radiation source, K is the free space path loss factor, ε is the path loss index, m_p represents the position of a certain radiation source, $\|\cdot\|$ represents the Euclidean distance between two vectors, and W_{m_i} is the shadow fading at m_i that obeys the lognormal distribution and satisfies the standard deviation of σ [22].

2.3 Problem Model

For the dynamic spectrum situation completion scenario, monitoring sensors are deployed on a two-dimensional geographical area of an $a \times b$ equidistant grid, and these sensors monitor the surrounding spectrum situation. At time t, the spectrum data use a matrix $\mathrm{X}_t \in \mathbb{R}^{a\times b}$, which is modeled as a three-dimensional spectrum tensor $\mathcal{X} \in \mathbb{R}^{a\times b\times t}$, as shown in Fig. 3.

The X and Y axes represent the spatial position, and the Z axis represents the movement time of the radiation source. The white cubes indicate missing spectrum data, and the blue cubes indicate the observed spectrum data information. In a complex electromagnetic environment, due to cost, the number of deployed monitoring sensors is limited; as a result, the collected spectrum data are often incomplete. Accurate spectrum map construction requires using many sensors. To reduce time and cost, a tensor completion algorithm must be applied to recover spectrum data from limited sensors.

The TR factors corresponding to the TR decomposition representation are found from the observation items of the incomplete spectrum tensor data to restore the missing items of the spectrum tensor data. The TR-based tensor completion model is:

$$\min_{[\mathcal{G}]} \left\| P_\Omega(\mathcal{T} - \Psi([\mathcal{G}])) \right\|_{\mathrm{F}}^2 \quad (3)$$

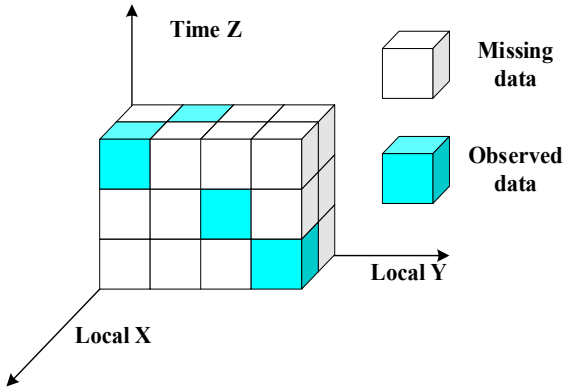

Fig. 3. Modeling of missing spectrum tensors.

where $\|\cdot\|_{\mathrm{F}}$ represents the Frobenius norm of the tensor, Ω represents the set of spectrum data observation items, $P_\Omega(\cdot)$represents the mapping under Ω, $\mathcal{T}$ represents the spectrum tensor data to be completed, and $\Psi([\mathcal{G}])$ represents the approximate spectrum tensor data generated by TR factors $[\mathcal{G}]$.

3. Spectrum Map Construction Method Based on Dynamic Window Size Tensor Ring Low-Rank Factors

3.1 Spectrum Map Generation Model Based on Tensor Ring Low-Rank Factors

To reduce the computational complexity of the traditional tensor completion methods, the low-rank constraint is imposed on the two rank-modes of the TR factors; that is, the expansion of the TR factors along mode-1 and mode-3 is denoted as $\sum_{n=1}^{N}\left\|\mathrm{G}_{(1)}^{(n)}\right\|_* + \sum_{n=1}^{N}\left\|\mathrm{G}_{(3)}^{(n)}\right\|_*$. A spectrum map construction model based on tensor ring low-rank factors (TRLRF) is proposed:

$$\begin{aligned} &\min_{[\mathcal{G}],\mathcal{X}} \sum_{n=1}^{N}\sum_{i=1}^{3}\left\|\mathrm{G}_{(i)}^{(n)}\right\|_* + \frac{\lambda}{2}\left\|\mathcal{X} - \Psi([\mathcal{G}])\right\|_{\mathrm{F}}^2 \\ &\text{s. t. } P_\Omega(\mathcal{X}) = P_\Omega(\mathcal{T}) \end{aligned} \quad (4)$$

where $\|\cdot\|_*$ represents the matrix kernel norm, λ is the trade-off parameter, $\lambda > 0$, and $\mathcal{X}$ represents the target spectrum tensor data.

ADMM is used to solve the objective function of the spectrum map generation model based on TRLRF. Since the model variables are interdependent, by adding auxiliary variables $[\mathcal{M}]$, the optimization problem of the objective function can be re-expressed as:

$$\begin{aligned} &\min_{[\mathcal{M}],[\mathcal{G}],\mathcal{X}} \sum_{n=1}^{N}\sum_{i=1}^{3}\left\|\mathbf{M}_{(i)}^{(n,i)}\right\|_* + \frac{\lambda}{2}\left\|\mathcal{X} - \Psi([\mathcal{G}])\right\|_{\mathrm{F}}^2 \\ &\text{s. t. } \mathbf{M}_{(i)}^{(n,i)} = \mathrm{G}_{(i)}^{(n)}, n = 1,\ldots,N, i = 1,2,3, \\ &P_\Omega(\mathcal{X}) = P_\Omega(\mathcal{T}). \end{aligned} \quad (5)$$

The set $[\mathcal{M}] := \{\mathcal{M}^{(n,i)}\}_{n=1,i=1}^{N,3}$ represents the tensor sequence, which is the auxiliary variable of $[\mathcal{G}]$. Equal constraints of auxiliary variables are added to the Lagrangian equation to obtain the augmented Lagrangian function of the objective function:

$$\begin{aligned} & L([\mathcal{G}],\mathcal{X},[\mathcal{M}],[\mathcal{Y}]) \\ & = \sum_{n=1}^{N}\sum_{i=1}^{3}\left(\left\|\mathbf{M}_{(i)}^{(n,i)}\right\|_{*} + <\mathcal{Y}^{(n,i)}, \mathcal{M}^{(n,i)} - \mathcal{G}^{(n)}> + \frac{\mu}{2}\left\|\mathcal{M}^{(n,i)} - \mathcal{G}^{(n)}\right\|_{\mathrm{F}}^{2}\right) \\ & + \frac{\lambda}{2}\left\|\mathcal{X} - \Psi([\mathcal{G}])\right\|_{\mathrm{F}}^{2} \\ & \text{s.t. } P_{\Omega}(\mathcal{X}) = P_{\Omega}(\mathcal{T}) \end{aligned} \tag{6}$$

where $[\mathcal{Y}] := \{\mathcal{Y}^{(n,i)}\}_{n=1,i=1}^{N,3}$ is the set of Lagrange multipliers and $\mu > 0$ is the penalty parameter. For $n = 1,\cdots,N$, $i = 1,2,3$, $\mathcal{G}^{(n)}$, $\mathcal{M}^{(n,i)}$, and $\mathcal{Y}^{(n,i)}$ are independent of each other. Therefore, the update scheme for each variable is as follows.

$$\begin{aligned} \mathcal{G}_{+}^{(n)} = \mathrm{fold}_2[(\sum_{i=1}^{3}(\mu\mathbf{M}_{(2)}^{(n,i)} + \mathbf{Y}_{(2)}^{(n,i)}) + \\ \lambda\mathbf{X}_{<n>}\mathrm{G}_{<2>}^{(\neq n)})(\lambda\mathrm{G}_{<2>}^{(\neq n),\mathrm{T}}\mathrm{G}_{<2>}^{(\neq n)} + 3\mu\mathbf{I})^{-1}] \end{aligned} \tag{7}$$

where the folding operations of mode-2 unfoldings are defined as $\mathrm{fold}_2(\cdot)$, that is, the matrix folding tensorization operation. $\mathbf{I} \in \mathbb{R}^{R_n^2 \times R_n^2}$ is the identity matrix.

$$\mathcal{M}_{+}^{(n,i)} = \mathrm{fold}_i\left(D_{\frac{1}{\mu}}(\mathrm{G}_{(i)}^{(n)} - \frac{1}{\mu}\mathrm{Y}_{(i)}^{(n,i)})\right) \tag{8}$$

where $D_{\frac{1}{\mu}}(\cdot)$ is the singular value thresholding (SVT) [23] operation.

$$\mathcal{X}_{+} = P_{\Omega}(\mathcal{T}) + P_{\bar{\Omega}}(\Psi([\mathcal{G}])) \tag{9}$$

where $P_{\Omega}(\mathcal{T})$ represents the mapping of the spectrum data to be completed under the set of observation items, $\bar{\Omega}$ is the set of missing items of the spectrum data, and $P_{\bar{\Omega}}(\Psi([\mathcal{G}]))$ represents the mapping of the approximate spectrum tensor data generated by TR factors $[\mathcal{G}]$ under $\bar{\Omega}$. The target spectrum tensor data $\mathcal{X}$ are updated by inputting the observed spectrum data, and the TR factors $[\mathcal{G}]$ are updated at each iteration to approximate the missing items of the spectrum data.

$$\mathcal{Y}_{+}^{(n,i)} = \mathcal{Y}^{(n,i)} + \mu(\mathcal{M}^{(n,i)} - \mathcal{G}^{(n)}). \tag{10}$$

Additionally, the penalty parameter μ of the augmented Lagrangian function of the objective function is updated by $\mu_{+} = \max\{\rho\mu, \mu_{\max}\}$ in each iteration, where $1 < \rho < 1.5$ is a tuning hyperparameter.

First, the ADMM is used to solve the objective function of the TRLRF model, and the objective function is transformed into a convex optimization problem. Since the variables of the TRLRF model are interdependent, auxiliary variables are included to simplify the optimization. Second, by constructing the augmented Lagrangian function form of the objective function, the optimization problem of the objective function is transformed into multiple subproblems to be solved separately. Finally, each subproblem is solved sequentially to update the auxiliary variables, and the target spectrum tensor data are output after multiple iterations of convergence to better address missing data in the spectrum map and improve the construction accuracy of the spectrum map.

3.2 Dynamic Window Size

When the radiation source motion time is too large, the TRLRF algorithm is inefficient in constructing a spectrum map. To reduce the computational complexity of the TRLRF algorithm, a dynamic window mechanism [20] is introduced. The dynamic window size is β_t, and the spectrum data at the relevant moment are put into the β_t. The observed spectrum data $\mathrm{X}_{t-\beta_t+1},\cdots, \mathrm{X}_{t-1}, \mathrm{X}_t$ have a strong correlation. According to the literature [20], it is concluded that $\beta_t \geq 2$, that is, at least $2ab$ entries can be observed as shown in Fig. 4.

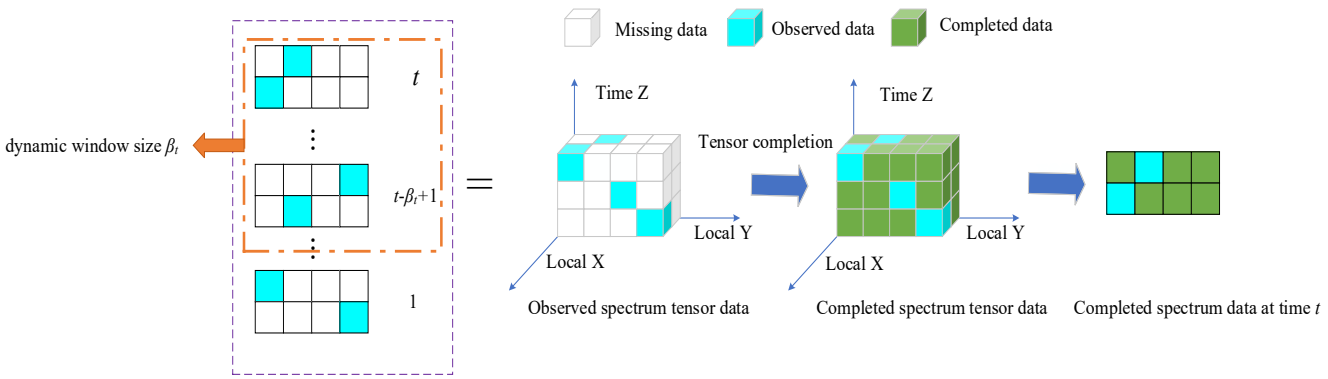

Fig. 4. Spectrum map construction process based on the DW-TRLRF algorithm.

Algorithm 1. DW-TRLRF algorithm

input: Spectrum tensor data to be completed $\mathcal{T}$, TR rank $\{R_n\}_{n=1}^{N}$ =3

output: Target spectrum tensor data $\mathcal{X}$ and TR factors $[\mathcal{G}]$

initialization: $n = 1,\ldots, N$, $i = 1,2,3$, $\mathcal{Y}^{(n,i)} = 0$, $\mathcal{M}^{(n,i)} = 0$, $\mu^0 = 1$, $\lambda = 5$, $\mu_{\max} = 100$, $\rho = 1.01$, $tol = 10^{-6}$, $k_{\max} = 300$, $\beta_t = 10$, $t = 200$

for $j = 1$ to $t - \beta_t + 1$ **do**

  while $j \le \beta_t$ **do**

    for $k = 1$ to $k_{\max}$ **do**

      $\mathcal{X}_{\text{last}} = \mathcal{X}$

      update $\{\mathcal{G}^{(n)}\}_{n=1}^{N}$ by（7）

      update $\{\mathcal{M}^{(n,i)}\}_{n=1,i=1}^{N,3}$ by（8）

      update $\mathcal{X}$ by（9）

      update $\{\mathcal{Y}^{(n,i)}\}_{n=1,i=1}^{N,3}$ by（10）

      $\mu = \max(\rho\mu, \mu_{\max})$

      If $\|\mathcal{X} - \mathcal{X}_{\text{last}}\|_{\text{F}} / \|\mathcal{X}\|_{\text{F}} < tol$, **break**

    end for

  end while

  while $j > \beta_t$ **do**

    Repeat steps 6, 7, 8, and 9 with only one iteration

  end while

end

The dynamic window size β_t at time t is calculated. Next, $\mathcal{G}^{(n)}$, $\mathcal{M}^{(n,i)}$, $\mathcal{X}$ and $\mathcal{Y}^{(n,i)}$ are updated. The TRLRF algorithm must perform multiple iterations of all the spectrum data observed at all times, which cannot meet the real-time requirements. Therefore, a spectrum map construction algorithm based on DW-TRLRF is proposed. When updating the spectrum data at the current time t, it only needs to use the spectrum data at the time $t - \beta_t$, $t - \beta_t + 1,\cdots, t - 1$ as the initial values of the DW-TRLRF algorithm, and the number of algorithm iterations is set to 1. Algorithm 1 summarizes the spectrum map construction process based on the DW-TRLRF algorithm.

3.3 Computational Complexity Analysis

For an N-dimensional tensor $\mathcal{X} \in \mathbb{R}^{I_1 \times I_2 \times \cdots \times I_N}$, the TR-rank is set to $R_1 = R_2 = \cdots = R_N = R$, and the dimension of each mode of the tensor is also set to be the same: $I_1 = I_2 = \cdots = I_N = I$. The computational complexity of the proposed TRLRF spectrum map construction algorithm is $O(NR^2I^N + NR^6)$, which is the same as that of the comparison algorithm TR-WOPT. The computational complexity of the TR-ALS algorithm is $O(PNR^4I^N + NR^6)$, where $0 < P < 1$, P represents the sampling rate. The computational complexity of the kriging interpolation algorithm is $O(S^3)$ [24], [25], where $S = P \times I^N$, S is the number of sampling points. The computational complexity of the proposed DW-TRLRF spectrum map construction algorithm is $O(I^2R^2)$.

Parameter	Numerical value
Target area	1000 m × 1000 m
Radiation source movement time	200 s
Radiation source movement speed	5 m/s
Radiation source emission power	[30 dBm, 26 dBm, 24 dBm]
Radiation source initial position	(500 m, 900 m), (900 m, 900 m), (900 m, 500 m)
Path loss index ε	2
Path loss factor K	10 dB
Shadow fading standard deviation (σ)	3 dB, 5 dB, 7 dB
Grid size	10 m × 10 m

Tab. 1. Simulation parameter settings.

4. Simulation Analysis

4.1 Simulation Settings

A summary of the parameter settings for the simulation data is provided in Tab. 1.

Three radiation sources are deployed in the target area of 1 km × 1 km, and the initial positions are randomly set to (500 m, 900 m), (900 m, 900 m) and (900 m, 500 m). The area is divided into 100 × 100 grids, each representing an area of 100 m^2, each grid with a different color to indicate the strength of the signal received by the grid. The simulation environment is shown in Fig. 5(a). Assuming that the radiation source moves at a speed of 5 m/s in the same direction, the spectrum maps after 100 seconds and 200 seconds of radiation source movement are shown in Fig. 5(b) and 5(c), respectively. Gudmundson's shadow fading model was used for statistical fading, and the standard deviation was 3 dB.

4.2 Dynamic Window Sizes Selection

To quantify the tensor completion algorithm performance, the root square error (RSE) [18] is used:

$$RSE\ [\text{dB}] = 10\log_{10}\frac{\|\hat{H} - H\|_2}{\|H\|_2} \tag{11}$$

where $\hat{H}$ is the completed spectrum tensor data, and H is the simulated original spectrum tensor data.

We use the same spectrum data with a spectrum data miss rate of 0.8 and a shadow fading standard deviation of 3 dB. As shown in Tab. 2, the running time of the constructed spectrum map increases with increasing dynamic window size, while the RSE first decreases with increasing dynamic window size. When the dynamic window size is 20, the RSE is the lowest, and when the dynamic window size is greater than 20, the RSE begins to increase. To better

Dynamic window size	RSE	Running time
5	−20.75 dB	2.75 s
10	−20.85 dB	3.50 s
15	−20.95 dB	5.82 s
20	−21.02 dB	6.31 s
25	−21.01 dB	7.38 s

Tab. 2. Comparison of RSE and running time with dynamic window size.

balance the construction accuracy and running time, we set the dynamic window size to 10.

4.3 Analysis of Spectrum Data Rank

To describe the characteristics of the rank of the spectrum tensor data, the spectrum data are preprocessed, expanded and decomposed into matrix form in the time dimension. Additionally, singular value decomposition (SVD) [26] is used to analyze the rank distribution of the spatial position of the radiation source that changes with the movement time and the distribution of the initial position rank under different shadow fading standard deviations.

In SVD, singular values are the elements on the diagonal matrix in the SVD of matrix **A**. Normalized singular values usually mean dividing the singular value by its largest singular value such that the large singular value equals 1. In particular, let the SVD of matrix **A** be:

$$\mathbf{A} = \mathbf{U}\mathbf{\Sigma}\mathbf{V}^{\mathrm{T}} \tag{12}$$

where **U** and $\mathbf{V}^{\mathrm{T}}$ are orthogonal matrices, respectively, and **Σ** are diagonal matrices whose elements on the diagonal are singular values, usually arranged in order from largest to smallest. The following formula calculates the normalized singular value σ'_i:

$$\sigma'_i = \frac{\sigma_i}{\sigma_{\max}} \tag{13}$$

where σ_i is the i-th element of the original singular value, and $\sigma_{\max}$ is the largest of the singular values.

Figure 6 shows the distribution of singular values in descending order after normalization. When the standard deviation of shadow fading is 3 dB, the three lines represent the spatial position of the radiation source at the initial moment, after 100 s of movement and after 200 s of movement. The spectrum map matrix singular value analysis curves are depicted. The rate of decrease in the singular value analysis curve is basically the same, which indicates that the rank of the spatial position of the radiation source remains relatively stable during motion.

Figure 7 shows the normalized singular values in descending order, and the three lines represent the singular value analysis curves of the spectrum map matrix with shadow fading standard deviations of 3 dB, 5 dB and 7 dB at the initial position, respectively. As shown in Fig. 7, as the standard deviation of shadow fading increases, the singular value analysis curve decreases more slowly; that is,

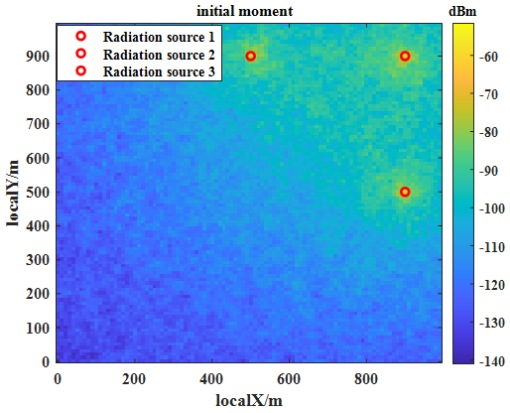

(a) Spectrum map generated by the radiation source at the initial moment.

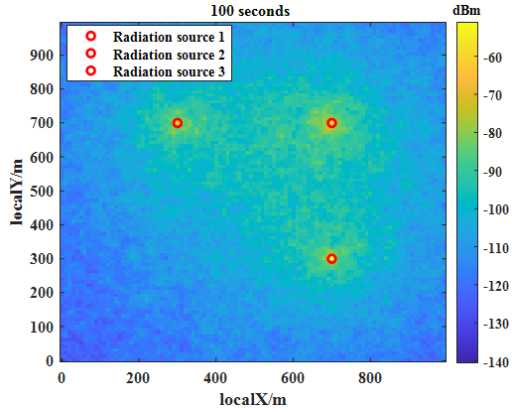

(b) Spectrum map generated after 100 seconds of radiation source motion.

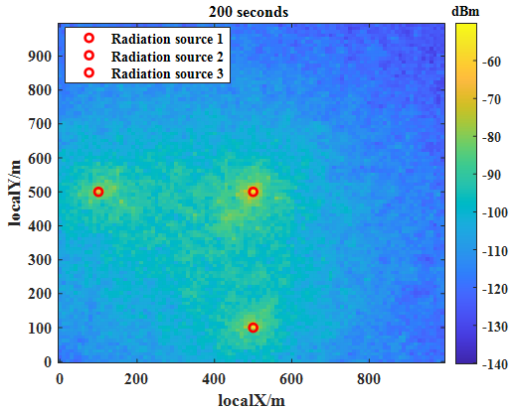

(c) Spectrum map generated after 200 seconds of radiation source motion.

Fig. 5. Spectrum map of the radiation source as it moves over time.

the spectrum map matrix's rank also increases, reducing the completion performance of the DW-TRLRF algorithm.

As shown from Fig. 6 and Fig. 7, the matrix singular value distribution of the signal reception intensity after expansion of the spectrum tensor is always concentrated in the first few singular values, indicating that the spectrum data have an approximate low-rank structure. Therefore, spectrum maps can be constructed using the DW-TRLRF algorithm.

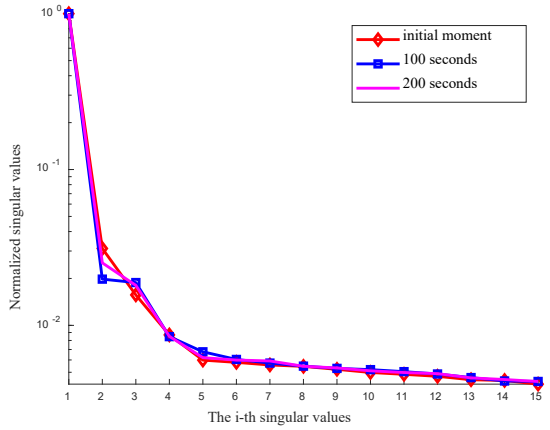

Fig. 6. Distribution of singular values of the spectrum matrix at different spatial locations.

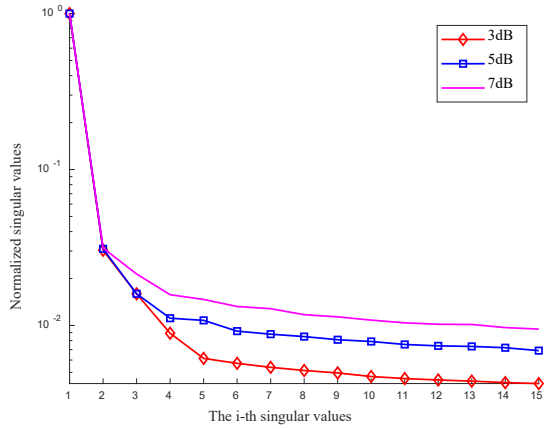

Fig. 7. Singular value distribution of the spectrum matrix under different shadow fading standard deviations.

4.4 Simulation Results and Discussion

In the target region of 1 km × 1 km, the radiation source motion time of 200 s is accounted for and modeled as a third-order spectrum tensor, as shown in Fig. 8(a). The size of the spectrum tensor data is 100 × 100 × 200. The X-axis and Y-axis represent the target region, and the Z-axis represents the movement time of the radiation source. Assuming that the missing rate of the spectrum data is 70%, the acquired signal intensity is displayed in different colors, and the missing spectrum tensor data are shown in Fig. 8(b). The spectrum tensor data completed by the DW-TRLRF algorithm are shown in Fig. 8(c). As shown in Fig. 8, the DW-TRLRF algorithm has excellent completion performance.

Figure 9 compares and analyzes the spectrum map construction accuracy of five algorithms based on different shadow fading standard deviations of simulation data, including TR-ALS, TR-WOPT, Kriging, TRLRF and DW-TRLRF. It shows that when the spectrum data missing rate is 0.2 to 0.8 and the shadow fading standard deviation is 3 dB, the average RSE of the spectrum map constructed by the DW-TRLRF algorithm is lower than that of TR-ALS, TR-WOPT, Kriging and TRLRF, reducing by 18.41%, 19.13%, 12.41% and 4.54%, respectively. The shadow fading standard deviation is 5 dB, reducing by 14.27%, 14.63%, 12.97% and 1.08%, respectively. The shadow fading standard deviation is 7 dB, reducing by 13.12%, 13.26%, 13.53% and 0.01%, respectively.

A time test is conducted on an i9-12900H CPU with 16 GB RAM, as shown in Fig. 10. When the spectrum data missing rate is 0.2 to 0.8, and the shadow fading standard

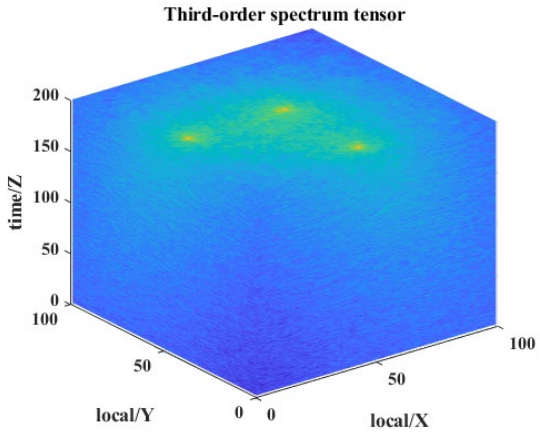

(a) Third-order spectrum tensor data.

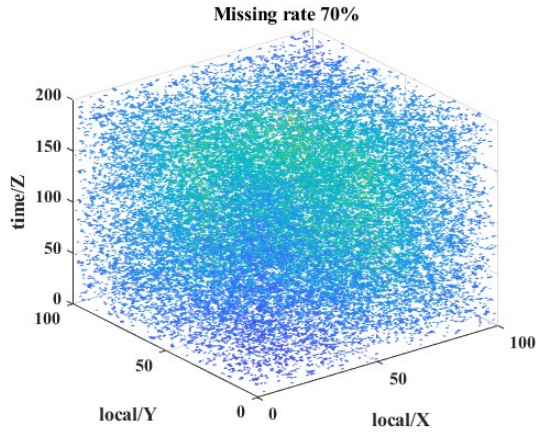

(b) Spectrum tensor data with a missing rate of 70%.

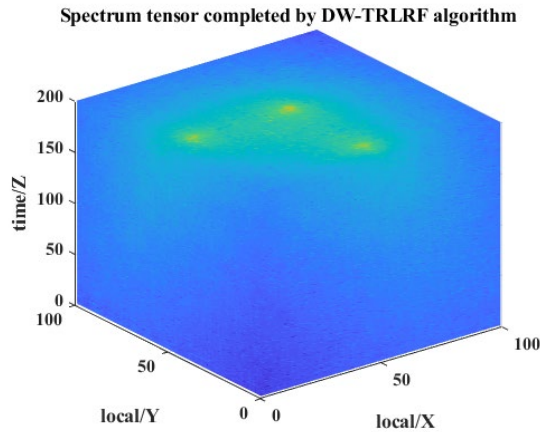

(c) Spectrum tensor data completed by the DW-TRLRF algorithm.

Fig. 8. Schematic diagram of the completion process of spectrum tensor data.

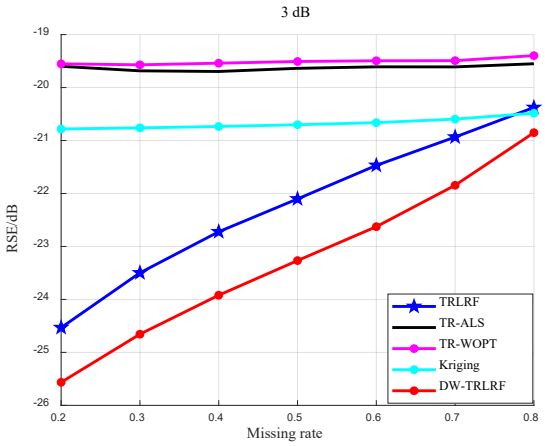

(a) The standard deviation of shadow fading is 3 dB.

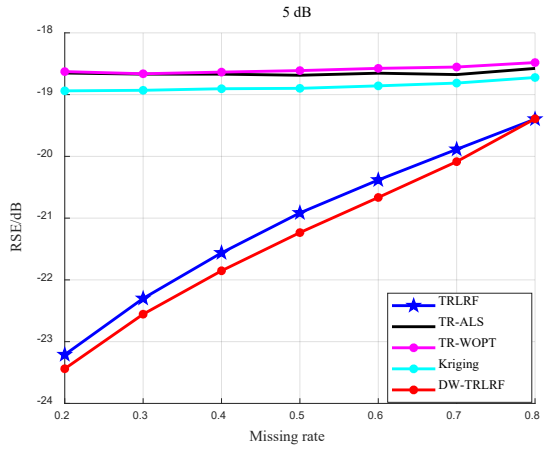

(b) The standard deviation of shadow fading is 5 dB.

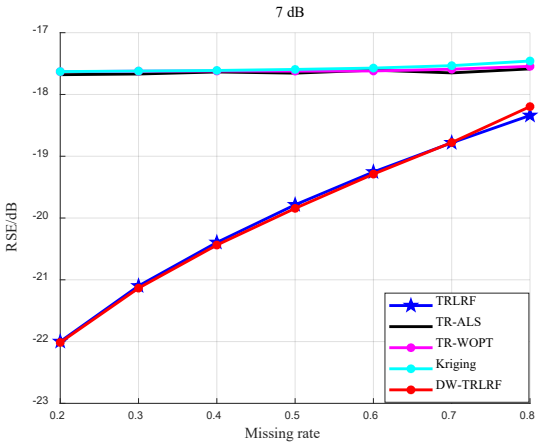

(c) The standard deviation of shadow fading is 7 dB.

Fig. 9. Comparison of RSE performance with spectrum data missing rate.

deviation is 3 dB, DW-TRLRF performs better than TR-ALS, TR-WOPT, Kriging and TRLRF in spectrum map construction, reducing the running time by an average of 39.85%, 94.1%, 99.67% and 86.75%, respectively.

By adding a dynamic window mechanism based on the TRLRF algorithm, DW-TRLRF can make full use of the temporal and spatial correlation characteristics of observation data and gradually eliminate the data outside the

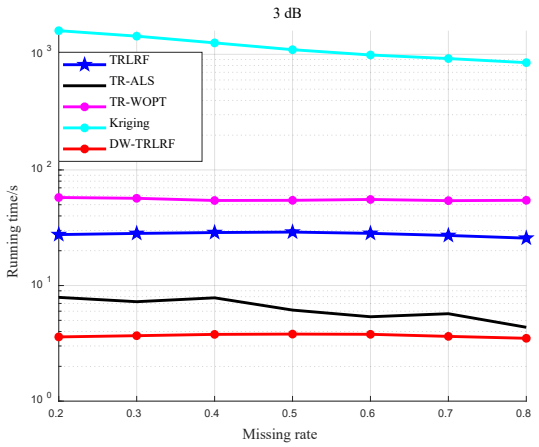

Fig. 10. Comparison of running times for constructing spectrum maps.

dynamic window size. Simulation results demonstrated that the running time was significantly reduced, and the current spectrum situation could be estimated more timely. The quick spectrum map construction with the proposed algorithm makes it more suitable for applications with timely construction requirements, such as searching the black flight of drones and managing unmanned aerial vehicle (UAV) activities for airspace safety.

To be more adaptive in different environments, the size of the dynamic window should be optimized before application to balance RSE and running time. Moreover, more research is needed to find the best dynamic window size.

5. Conclusions

In this paper, a spectrum map construction algorithm based on TRLRF is designed to solve the problem of real-time construction of dynamic spectrum situations. Through TR decomposition, TR factors are found from incomplete spectrum data to estimate the missing spectrum data and improve the spectrum map construction accuracy. In order to make full use of the correlation of spatial-temporal spectrum data, a dynamic window mechanism is introduced to reduce the computational complexity, and a spectrum map construction algorithm based on DW-TRLRF is proposed, which can quickly construct spectrum maps. The simulation results show that when the spectrum data missing rate is 0.2 to 0.8, and the shadow fading standard deviation is 3 dB, the RSE of the DW-TRLRF algorithm is reduced by 12.41% on average compared with the classic Kriging interpolation method, and the running time of constructing spectrum map is reduced by 99.67% on average, which significantly reduces the computational complexity. The proposed algorithm can better meet the requirements of dynamic spectrum situation scenario construction.

Since the spectrum environment varies with time and location, the correlation among the observed data decreases. Completing the spectrum map with all observed data is neither necessary nor preferable, especially consid-

ering the high computational complexity. Therefore, introducing a dynamic window mechanism to put highly relevant spectrum data into a complete system can quickly and accurately construct spectrum maps, which play a crucial role in improving the efficiency of spectrum management.

Acknowledgments

This work was supported by the National Natural Science Foundation of China No. 62131005.

References

[1] LEE, D., KIM, S. J., GIANNAKIS, G. B. Channel gain cartography for cognitive radios leveraging low rank and sparsity. *IEEE Transactions on Wireless Communications*, 2017, vol. 16, no. 9, p. 5953–5966. DOI: 10.1109/TWC.2017.2717822

[2] ZHAO, Y., ZHU, Q., LIN, Z., et al. Temporal prediction for spectrum environment maps with moving radiation sources. *IET Communications*, 2023, vol. 17, no. 5, p. 538–548. DOI: 10.1049/cmu2.12560

[3] LU, J., ZHA, S., HUANG, J., et al. The iterative completion method of the spectrum map based on the difference of measurement values. In *2018 IEEE 3rd International Conference on Signal and Image Processing* (*ICSIP*). Shenzhen (China), 2018, p. 255–259. DOI: 10.1109/SIPROCESS.2018.8600488

[4] WANG, C., WU, Y., ZHOU, F., et al. Accurate spectrum map construction using an intelligent frequency-spatial reasoning approach. In *IEEE Global Communications Conference (GLOBECOM 2022)*. Rio de Janeiro (Brazil), 2022, p. 3460–3465. DOI: 10.1109/GLOBECOM48099.2022.10001024

[5] ZHANG, G. Y., WANG, J., CHEN, X. N., et al. Spectrum situation generation from sparse spatial sampling: Model and algorithm (in Chinese). *Scientia Sinica Information*, 2022, vol. 52, p. 2011–2036. DOI: 10.1360/SSI-2021-0382

[6] CHEN, G., LIU, Y., ZHANG, T., et al. A graph neural network based radio map construction method for urban environment. *IEEE Communications Letters*, 2023, vol. 27, no. 5, p. 1327–1331. DOI: 10.1109/LCOMM.2023.3260272

[7] SUN, H., CHEN, J. Propagation map reconstruction via interpolation assisted matrix completion. *IEEE Transactions on Signal Processing*, 2022, vol. 70, p. 6154–6169. DOI: 10.1109/TSP.2022.3230332

[8] BOCCOLINI, G., HERNANDEZ-PENALOZA, G., BEFERULL-LOZANO, B. Wireless sensor network for spectrum cartography based on kriging interpolation. In *IEEE 23rd International Symposium on Personal, Indoor and Mobile Radio Communications (PIMRC).* Sydney, (Australia), 2012, p. 1565 to 1570. DOI: 10.1109/PIMRC.2012.6362597

[9] SHEN, F., WANG, Z., DING, G., et al. 3D compressed spectrum mapping with sampling locations optimization in spectrum-heterogeneous environment. *IEEE Transactions on Wireless Communications*, 2022, vol. 21, no. 1, p. 326–338. DOI: 10.1109/TWC.2021.3095342

[10] ZHANG, G., FU, X., WANG, J., et al. Spectrum cartography via coupled block-term tensor decomposition. *IEEE Transactions on Signal Processing*, 2020, vol. 68, p. 3660–3675. DOI: 10.1109/TSP.2020.2993530

[11] BASSER, P. J., MATTIELLO, J., LEBIHAN, D. MR diffusion tensor spectroscopy and imaging. *Biophysical Journal*, 1994, vol. 66, no. 1, p. 259–267. DOI: 10.1016/S0006-3495(94)80775-1

[12] LEBIHAN, D., MANGIN, J. F., POUPON, C., et al. Diffusion tensor imaging: Concepts and applications. *Journal of Magnetic Resonance Imaging: An Official Journal of the International Society for Magnetic Resonance in Medicine*, 2001, vol. 13, no. 4, p. 534–546. DOI: 10.1002/jmri.1076

[13] ACAR, E., DUNLAVY, D. M., KOLDA, T. G., et al. Scalable tensor factorizations for incomplete data. *Chemometrics and Intelligent Laboratory Systems*, 2011, vol. 106, no. 1, p. 41–56. DOI: 10.1016/j.chemolab.2010.08.004

[14] YUAN, L., LI, C., MANDIC, D., et al. Tensor ring decomposition with rank minimization on latent space: An efficient approach for tensor completion. In *Proceedings of the AAAI conference on Artificial Intelligence*. Honolulu (USA), 2019, vol. 33, no. 1, p. 9151–9158. DOI: 10.1609/aaai.v33i01.33019151

[15] HAN, D. R. A survey on some recent developments of alternating direction method of multipliers. *Journal of the Operations Research Society of China*, 2022, vol. 10, p. 1–52. DOI: 10.1007/s40305-021-00368-3

[16] WANG, W., AGGARWAL, V., AERON, S. Efficient low rank tensor ring completion. In *Proceedings of the IEEE International Conference on Computer Vision*. Venice (Italy), 2017, p. 5697 to 5705. DOI: 10.1109/iccv.2017.607

[17] YUAN, L., CAO, J., ZHAO, X., et al. Higher-dimension tensor completion via low-rank tensor ring decomposition. In *2018 Asia-Pacific Signal and Information Processing Association Annual Summit and Conference* (*APSIPA ASC*). Honolulu, (USA), 2018, p. 1071–1076. DOI: 10.23919/APSIPA.2018.8659708

[18] TANG, M., DIND, G., WU, Q., et al. A joint tensor completion and prediction scheme for multi-dimensional spectrum map construction. *IEEE Access*, 2016, vol. 4, p. 8044–8052. DOI: 10.1109/ACCESS.2016.2627243

[19] TANG, M., DING, G., XUE, Z., et al. Multi-dimensional spectrum map construction: A tensor perspective. In *2016 8th International Conference on Wireless Communications* & *Signal Processing* (*WCSP*). Yangzhou (China), 2016, p. 1–5. DOI: 10.1109/WCSP.2016.7752600

[20] ZHANG, G., WANG, J., PENG, Q., et al. Dynamic spectrum cartography via canonical polyadic tensor decomposition. *Signal Processing*, 2021, vol. 188, p. 1–13. DOI: 10.1016/j.sigpro.2021.108208

[21] DING, Z., ZHANG, J., LIU, Y., et al. Spectrum map construction based on optimized sensor selection and adaptive kriging model. *Radioengineering*, 2022, vol. 31, no. 3, p. 422–430. DOI: 10.13164/re.2022.0422

[22] GUDMUNDSON, M. Correlation model for shadow fading in mobile radio systems. *Electronics Letters*, 1991, vol. 27, no. 23, p. 2145–2146. DOI: 10.1049/el:19911328

[23] CAI, J. F., CANDES, E. J., SHEN, Z. A singular value thresholding algorithm for matrix completion. *SIAM Journal on Optimization*, 2010, vol. 20, no. 4, p. 1956–1982. DOI: 10.1137/080738970

[24] SRINIVASAN, B. V., DURAISWAMI, R., MURTUGUDDE, R. *Efficient Kriging for Real-Time Spatio-Temporal Interpolation.* 8 pages. [Online] Cited 2010-01-18. Available at: https://api.semanticscholar.org/CorpusID:12111470

[25] HU, W., LIU, H., PENG, C., et al. A construction technology of electromagnetic spectrum map based on the kriging algorithm (in Chinese). *Journal of Air Force Engineering University* (*Natural Science Edition*), 2022, vol. 23, no. 3, p. 26–33. DOI: 10.3969/j.issn.1009-3516.2022.03.005

[26] AHARON, M., ELAD, M., BRUCKSTEIN, A. K-SVD: An algorithm for designing overcomplete dictionaries for sparse representation. *IEEE Transactions on Signal Processing*, 2006, vol. 54, no. 11, p. 4311–4322. DOI: 10.1109/TSP.2006.881199

About the Authors ...

Yihan HU is currently a master student at the School of Electronics and Information Engineering, Nanjing University of Information Science and Technology, Nanjing, China. His research interests include spectrum map construction methods.

Jianzhao ZHANG received the Ph.D. degree in Communication Engineering from the PLA University of Science and Technology, Nanjing, China, in 2012. He is currently an Associate Researcher in the Sixty-third Research Institute, National University of Defense Technology, Nanjing, China. His research interests include spectrum environment cognition and smart spectrum management.

Yongxiang LIU (corresponding author: The Sixty-third Research Institute, National University of Defense Technology, Nanjing, China, 210007; E-mail: lyx63s@163.com) received the M.S. degree in Communications and Information Systems from the Institute of Communications Engineering, Nanjing, China, in 1999. He is currently a Professor in the Sixty-third Research Institute, National University of Defense Technology, Nanjing, China. His research interests include wireless communications, spectrum management, and communication anti-jamming.

Guangjie LIU received the Ph.D. degree in Control Science and Engineering from the Nanjing University of Science and Technology, Nanjing, China, in 2006. He is currently a Professor and doctoral supervisor at the School of Electronics and Information Engineering, Nanjing University of Information Science and Technology, Nanjing, China. His research interests include intelligent networks and communication security.

Guokai CHEN received his B.S degree in Measurement and Control Technology from the National University of Defense Technology in 2019. He is currently a Ph.D. student in the College of Intelligence Science at the National University of Defense Technology. His research interests include spectrum map construction methods and spectrum map-based localization.